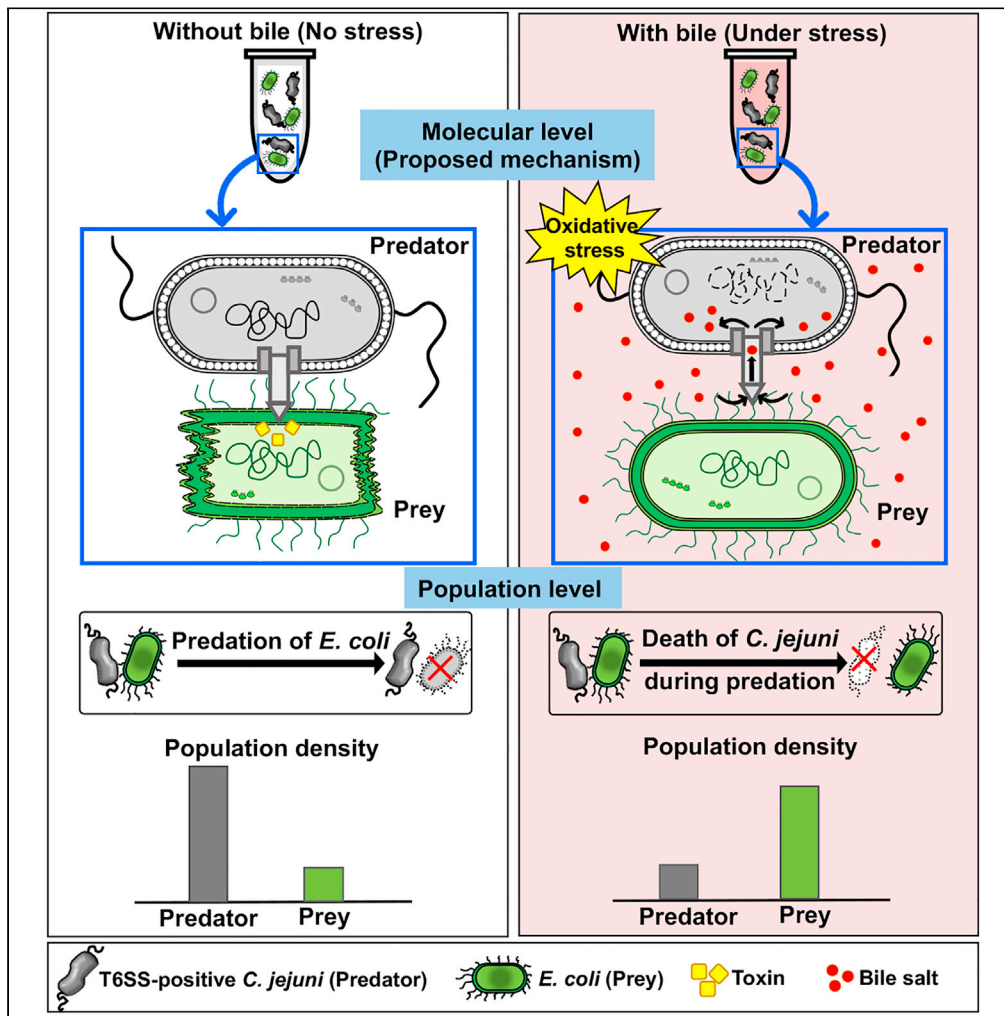


Article

The cost of bacterial predation via type VI secretion system leads to predator extinction under environmental stress



Subhadeep Gupta,
Soumyadipta Ray,
Afruja Khan,
Arkaprabha China,
Dipjyoti Das,
Amirul Islam Mallick

dipjyoti.das@iiserkol.ac.in (D.D.)
amallick@iiserkol.ac.in (A.I.M.)

Highlights
Campylobacter jejuni uses Type VI secretion system (T6SS) to kill prey bacteria

Under bile salt stress, activated T6SS may promote bile salt uptake and DNA damage

T6SS-dependent predation by *C. jejuni* thus entails a “predation cost” under stress

The predation cost leads to predator extinction and host defense against *C. jejuni*



Article

The cost of bacterial predation via type VI secretion system leads to predator extinction under environmental stress

Subhadeep Gupta,¹ Soumyadipta Ray,¹ Afruja Khan,¹ Arkaprabha China,¹ Dipjyoti Das,^{1,2,*} and Amirul Islam Mallick^{1,2,3,*}

SUMMARY

As a common gut pathogen, *Campylobacter jejuni* (*C. jejuni*) harbors the Type VI Secretion System (T6SS) that injects toxic effectors into neighboring cells, modulating microbial competitions in the harsh gut environment. Using bile salt as a natural stressor and T6SS-positive *C. jejuni* as a predator, we show that T6SS activity could entail a cost during bacterial predation under environmental stress. Our data suggest bile salt influx and subsequent DNA damage due to the prey-driven activation of the T6SS. We further combined experiments and mathematical modeling to explore how the stress-induced “predation cost” determines ecological outcomes. Consistent with a population-dynamics model, we found predator extinction above a critical bile salt concentration and prey-predator coexistence below this level. Moreover, we utilized the predation cost as an effective strategy facilitating host defense against *C. jejuni* infection. Together, we elucidate how predator dominance versus extinction emerges from the interplay between environmental stress and the T6SS machinery.

INTRODUCTION

The role of gut microbiota in modulating host adaptability largely relies on microbial coexistence and predator-prey relationships in a dynamic micro-environment (Priya and Blekhman, 2019; David et al., 2014; Chen et al., 2019; Hornung et al., 2018). In addition to the intrinsic mechanisms of gut bacteria to evade innate host defenses, their self-survival in the harsh gut environment depends on bacterial secretion systems (Green and Meccas, 2016; Desvaux and Hébraud, 2006; Hersch et al., 2020; Abby et al., 2016). Particularly, the bacterial Type VI Secretion System (T6SS) secretes a vast repertoire of effector molecules targeting prey or competing bacteria in a contact-dependent manner (Dörr and Blokesch, 2018; Basler et al., 2013; Mougous et al., 2006; Schell et al., 2007; Yu and Lai, 2017). The T6SS is present in nearly 25% of gram-negative pathogens, including *Pseudomonas aeruginosa* (Mougous et al., 2006), *Vibrio cholerae* (Basler et al., 2012; Fast et al., 2018), *Burkholderia mallei* (Schwarz et al., 2010), *Salmonella enterica* (Wang et al., 2011), and *Campylobacter jejuni* (*C. jejuni*) (Noreen et al., 2018; Lertpiriyapong et al., 2012; Sha et al., 2013). A functional T6SS facilitates bacterial predation (Cianfanelli et al., 2016), host cell adherence, and invasion (Lertpiriyapong et al., 2012), conferring a selective advantage to the predator over other prey bacteria within the same environmental niche (Dörr and Blokesch, 2018; Wood et al., 2020). However, an important question is how molecular activities of T6SS at a cellular level translate into ecological outcomes at a population level. For instance, the T6SS functionality at physiological conditions can affect population-level phenomena like extinction, coexistence, or over-proliferation of a pathogen, which, in turn, dictate the epidemiological upshot. Although the structure, function, and localization of T6SS are known to some extent, there is still much to learn about the molecular mechanisms of T6SS-mediated predation, environmental effects on those mechanisms, and their potential application in improving gut health.

Considering the structural similarities between effector proteins of *C. jejuni* T6SS with other gram-negative bacteria (Wang et al., 2011), we chose *C. jejuni* as a model to study T6SS-mediated predation. Intriguingly, in contrast to gastroenteritis in humans, *C. jejuni* remains commensal in chickens' gut with little or no pathological outcomes (Humphrey et al., 2014; Awad et al., 2018; Newell and Fearnley, 2003). However, in light of the cytotoxic function of T6SS, the question remains how a T6SS-positive (T6SS+ve) *C. jejuni* can coexist with other resident microbes.

¹Department of Biological Sciences, Indian Institute of Science Education and Research Kolkata, Mohanpur, Nadia, West Bengal, 741246, India

²These authors contributed equally

³Lead contact

*Correspondence: dipjyoti.das@iiserkol.ac.in (D.D.), amallick@iiserkol.ac.in (A.I.M.)

<https://doi.org/10.1016/j.isci.2021.103507>



To this end, we used a particular chicken isolate of *C. jejuni* harboring T6SS as a predator and a non-pathogenic laboratory strain of *Escherichia coli* (*E. coli*) (DH5 α) as prey. As expected, we found that T6SS+ve *C. jejuni* can efficiently kill *E. coli* with marked morphological changes. Since the gut environment is known to modulate bacterial fitness (Hornung et al., 2018), we further re-evaluated the prey-predator interaction in a harsh environment, using bile salt as a natural stressor of the gut.

Of interest, in the presence of prey and for a wide range of bile salt concentrations (0.05%–0.25%), T6SS+ve *C. jejuni* exhibited a significant decrease in number, whereas T6SS-negative (T6SS-ve) *C. jejuni* remains unaffected. We thus hypothesized a prey-driven activation of T6SS, which may act as a trans-membrane channel allowing the influx of bile salt into bacterial cells. Since *Campylobacter* multidrug efflux pump (CmeABC) is known to promote efflux of several antimicrobial agents, including bile salt, we tested our hypothesis by analyzing the transcriptional profile of *cmeABC* genes (Lin et al., 2002; Grinnage-Pulley et al., 2016). We indeed found a marked up-regulation of *cmeABC* genes and subsequent DNA degradation of T6SS+ve *C. jejuni* in the presence of prey.

Taken together, T6SS-mediated predation under bile salt stress may entail a predation cost at the population level, leading to a possibility where predators can die faster than the prey. To explore this, we developed a mathematical model incorporating predator-prey interactions with a “cost” of predation under environmental stress. This model identified distinct possible regimes, such as the extinction of prey or predator and the coexistence of both, when bile salt concentration is varied. Consistent with the prediction, we found that T6SS+ve predators become extinct above a critical bile salt concentration, whereas predator and prey coexist below that level. Thus, the interplay of molecular machinery and environmental stress leads to distinct outcomes: at favorable conditions, predators make the prey extinct, and at stress conditions, predators themselves become extinct.

To see whether the predation cost under stress could be translated as a host defense strategy against *C. jejuni* infection, we studied *in vitro* *C. jejuni* invasion in the presence of prey and bile salt, using human intestinal epithelial cells (INT407 cells). We provide direct evidence that bile salt stress and high prey density effectively reduce the intra-cellular counts of *C. jejuni*. In principle, this result highlights the possibility of a promising alternative in controlling bacterial pathogenesis by manipulating the ecological parameters in the gut without antimicrobials.

RESULTS

Isolation, identification, and functional characterization of T6SS+ve *C. jejuni*

To examine the role of T6SS in *C. jejuni* predation, we isolated *C. jejuni* from the cecal content of broiler chickens following standard morphological, biochemical, and molecular methods of identification (see Figures 1A, S1A–S1D, and supplemental information for details). Since broilers remain an affordable source of animal proteins for developing countries (Beski et al., 2015), we specifically chose to use *C. jejuni* of chicken origin to study T6SS-mediated microbial interactions. Based on the presence of major T6SS genes (*hcp*, *vasC*, *vasD*, *vasE*, and *vasK*), we found 8 genotypes of the 32 *C. jejuni* isolates to be positive for all the genes (Tables S1 and S2). We report here a detailed study of predation ability and stress response with a T6SS+ve isolate (2B4) and a T6SS-ve isolate (3A1); nevertheless, other isolates were also tested for the generality of some key conclusions. Since Hemolysin co-regulated protein (Hcp) is considered as a major effector protein secreted by a functional T6SS (Noreen et al., 2018; Lertpiriyapong et al., 2012; Singh et al., 2019), the presence of Hcp was confirmed by western blot in the culture supernatant of T6SS+ve isolates (Figure 1B) and the amount of the protein was quantified by indirect ELISA (Figures 1C and 1D).

Predator-prey interactions in co-cultures of *C. jejuni* and *E. coli*

We used a T6SS+ve isolate as a model predator, while T6SS-ve *C. jejuni* served as a negative control (Figure 2A). To visualize predator-prey interaction in a co-culture, we used a laboratory strain of *E. coli* (DH5 α) transformed with pTurboGFP-B plasmid as prey (see green *E. coli* cells in Figures 2A and S1E). To determine whether *C. jejuni* T6SS could prompt changes in its prey, we captured microscopy images and found elongated morphology (~7.8 μ m in length) of prey. In comparison, such difference was not found in *E. coli* when cultured with T6SS-ve *C. jejuni* (~3.8 μ m). These data (Figure 2B) indicate delayed cell division of the prey under predation stress.

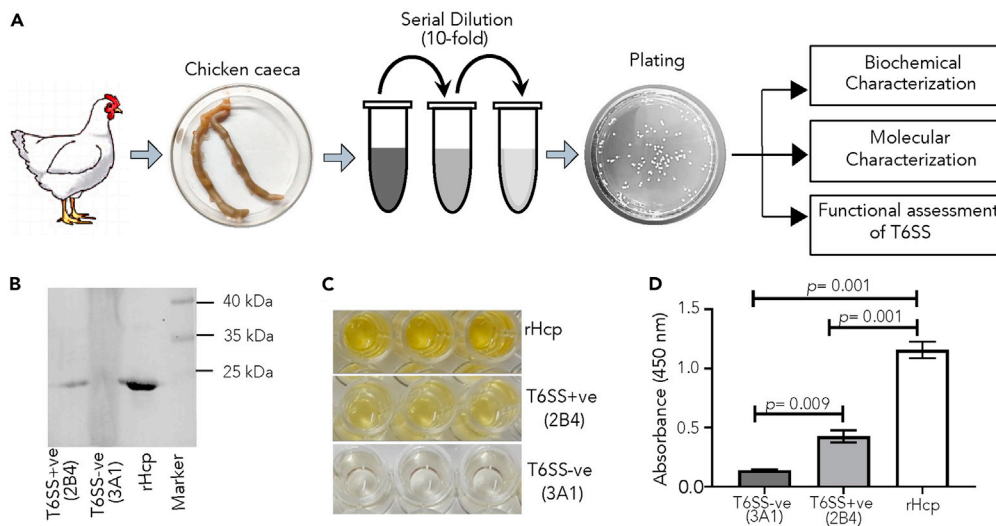


Figure 1. Isolation, identification, and functional characterization of T6SS+ve *C. jejuni*

(A) Schematic flowchart of sampling and identification of *C. jejuni*. Sample collected from chicken caeca was processed and screened based on morphological, biochemical (catalase, oxidase, hippuricase), and molecular methods (16S rRNA, *hipO*, *ciaB*, and *cadF*) of identification.

(B–D) The presence of Hcp was detected in the culture supernatant by western blot analysis (B) and quantified by indirect ELISA (C and D). Probing with an anti-Hcp antibody showed a protein band at 20 kDa size that corresponds to Hcp. Error bars represent standard deviation (mean \pm SD).

As the *Filamenting temperature-sensitive mutant Z* (*ftsZ*) gene is responsible for the cytokinesis of *E. coli* (Margolin, 2005), we further analyzed its expression by semi-quantitative RT-PCR (Figure S1G). The fold change data, calculated with respect to the control group (only *E. coli*), suggest down-regulated *ftsZ* gene expression (~0.7 fold) in the presence of predators (see Figure 2C). Furthermore, field emission scanning electron microscopy (FESEM) images also revealed the elongation and cell wall damage at the polar ends of *E. coli* cells. However, no such morphological changes were found in *E. coli* co-cultured with a T6SS-ve *C. jejuni* isolate (Figure 2D), suggesting T6SS-mediated prey killing. Furthermore, the prey cell density was substantially lower at 10 h post incubation with T6SS+ve *C. jejuni* than the control (with T6SS-ve *C. jejuni*) (Figure 2E). In summary, the T6SS+ve *C. jejuni* seems to act as an efficient killer, which is in line with the established role of T6SS in bacterial predation (Basler et al., 2013), whereas T6SS-ve *C. jejuni* fails to target prey cells.

We further characterized the T6SS+ve and T6SS-ve isolates based on several phenotypic and structural compositions for putative virulence repertoires such as motility, biofilm formation, carbohydrate, and lipo-oligosaccharides contents. We found no noticeable difference among the isolates (Figure S2). This may exclude the possible involvement of other genes in the predation ability of T6SS+ve *C. jejuni*. Furthermore, when tested for Hcp as a hallmark of functional T6SS, we found that Hcp secretion was proportional to the available number of the prey population, indicating a prey-driven enhancement of T6SS activation (see Figure S1F).

A model predicting temporal dynamics of predator-prey populations

We further developed a simple mathematical model to explore how T6SS-mediated killing of prey shapes the population dynamics (Figure 3A). At an instant (*t*), the predator and prey densities (denoted by *P* and *N*, respectively) can be described by the following equations.

$$\frac{dP}{dt} = r_P P \left(1 - \frac{P}{K_P} \right) \quad (\text{Equation 1})$$

$$\frac{dN}{dt} = r_N N \left(1 - \frac{N}{K_N} \right) - \alpha NP \quad (\text{Equation 2})$$

Here, r_P and r_N are birth rates and while K_P and K_N are carrying capacities of the predator and prey, respectively. Both populations grow logistically in the absence of inter-species interaction and ultimately saturate

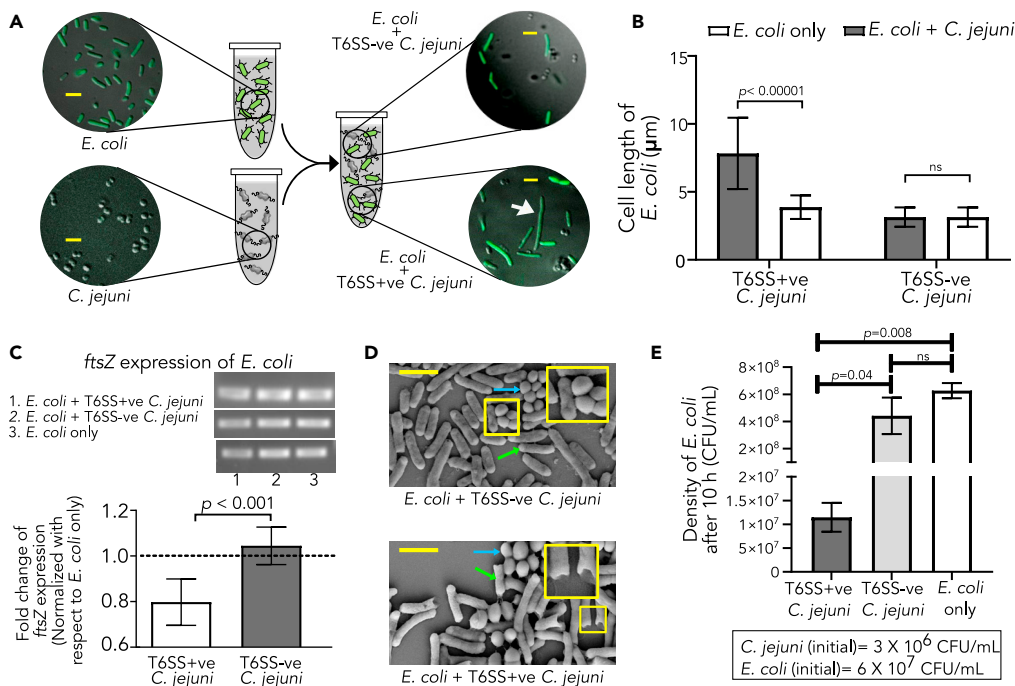


Figure 2. Effect of T6SS-mediated predation of *C. jejuni* on morphology and growth profiles of prey

(A) A schematic of predator-prey interactions in co-cultures is shown along with representative images (Epi-fluorescence) of GFP-expressing *E. coli* and T6SS+ve *C. jejuni* (prey cells in green and predators in gray). The arrow indicates an elongated *E. coli* cell, suggesting possible growth arrest under predation stress. Scale bar: 4 μm .

(B) Significant increase in mean length of *E. coli* in the presence of T6SS+ve *C. jejuni* compared with T6SS-ve *C. jejuni*.

(C) Gel images showing relative expression of *ftsZ* gene of *E. coli* as a key marker for cell division (top). Approximately 0.7-fold decrease in *ftsZ* gene expression (bottom) was noted in cells grown with T6SS+ve *C. jejuni* ($n = 7$).

(D) Distinct changes in *E. coli* morphology (shredded poles) in the presence of T6SS+ve *C. jejuni* under FESEM (inset, bottom). The blue and green arrows indicate *C. jejuni* and *E. coli* cells, respectively. Scale bar: 4 μm . In B-D, initial counts of *E. coli* and *C. jejuni* were 6×10^7 CFU/mL and 3×10^8 CFU/mL, respectively.

(E) Significant reduction in *E. coli* cell count (CFU/mL) in the presence of T6SS+ve *C. jejuni* at 10 h. Error bars represent standard deviation (mean \pm SD) ($n = 6$).

to their respective carrying capacities in the model. The second term in Equation 2 represents the predation, and α is the predation coefficient. Thus, α is a positive parameter for T6SS+ve *C. jejuni*, whereas it should be nearly zero for T6SS-ve *C. jejuni*. Our equations are distinct from the classical Lotka-Volterra equations applied to microbial communities since the predators do not seem to relish a direct metabolic advantage by killing their prey; instead, the prey killing may have evolved to achieve a niche/resource dominance in a dynamic environment. Hence, the predator's per capita growth rate is not dependent on prey density. However, the possibility of nutrient acquisition by the predator from the dead prey cannot be ruled out, although our model does not depend on such assumptions.

To test our model, we first extracted birth rates and carrying capacities from experiments with control groups, namely, *C. jejuni* or *E. coli* only (Figures S3A–S3C and Table S3). Next, we measured population densities (CFU/mL) from predator-prey co-cultures at different times. We found a reasonable agreement between the data and model prediction with a choice of predation coefficient, $\alpha = 7 \times 10^{-9}/\text{h}/(\text{CFU/mL})$ (see Figures 3B and 3C). The predation coefficient in other bacterial predator-prey systems satisfying Lotka-Volterra equations (such as *Bdellovibrio* and its prey) was reported as $\sim 10^{-12}/\text{h}$ at a very low prey density (Varon and Zeigler, 1978), which is orders of magnitude smaller than our value, indicating highly efficient killing via functional T6SS. Nevertheless, the extent of prey killing depends on the initial ratio of the predator to prey (Figure S3F). By using $\alpha = 0$, the model prediction also matched well with the population densities in co-cultures of *E. coli* and T6SS-ve *C. jejuni*, indicating almost no predation (Figures S3D and S3E). The validity of our model suggests that the predation depends on chance encounters between predator and prey (described as the product of prey and predator densities in Equation 2).

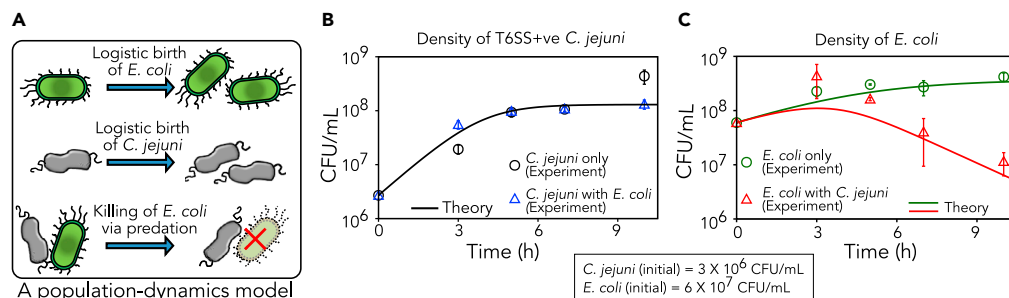


Figure 3. A model captures predator-prey population dynamics

(A) Schematic showing population-level processes on which our model is based (see Equations 1 and 2).

(B and C) Theoretical predictions (solutions of Equations 1 and 2) along with experimentally measured population densities over time. The temporal dynamics of T6SS+ve *C. jejuni* population were almost unaffected in the presence of prey (B), but the prey population steadily decreased at large times (C). Model parameters: $r_p = 1.0/\text{h}$, $r_N = 0.4/\text{h}$, $K_p = 1.3 \times 10^8 \text{ CFU/mL}$, $K_N = 3.7 \times 10^8 \text{ CFU/mL}$ (these were estimated from experiments, see Table S2), and $\alpha = 7 \times 10^{-9}/\text{h}$ (CFU/mL). Error bars represent standard deviation (mean \pm SD).

Bile salt-induced predation cost alters the prey-predator relationship

Since the intrinsic physicochemical composition of gut fluid helps to maintain homeostasis and contributes to microbial commensalism, we further asked how an altered environment affects the T6SS-mediated predation. As a major antimicrobial agent, bile salt contributes to the innate host defense against gut pathogens (Begley et al., 2005). Therefore, we reassessed the prey-predator interaction under stress induced by bile salt (a mixture of sodium cholate and sodium deoxycholate).

To this end, we first co-cultured *E. coli* and *C. jejuni* for 2 h followed by incubation in the presence of bile salt solution for an additional 5 h (Figure 4A). Furthermore, we systematically titrated the bile salt concentration (w/v) for assessing the effect of bile salt-induced stress on *C. jejuni* predation. As expected, the *C. jejuni* populations decreased steadily as bile salt concentrations were increased (Figures 4B and 4C). Strikingly, in the presence of prey, T6SS+ve *C. jejuni* exhibited a significant decrease in number for a range of bile salt concentrations (0.05%–0.25%), but the presence or absence of prey did not have any noticeable effect on T6SS-ve *C. jejuni* survival (see insets in Figures 4B and 4C). Moreover, this trend was observed in other isolates with similar genotypes (Figure S4), signifying a general functional aspect of T6SS under stress. These attributes suggest that prey-driven usage of T6SS promotes predator deaths as a unique response to bile salt stress. This stands in sharp contrast to the established positive role of T6SS in bacterial survival and adaptation to a harsh environment. Thus, we anticipate a prey-driven activation of T6SS machinery to facilitate intracellular entry of bile salt (Lertpiriyapong et al., 2012).

Since bile salt tolerance of *C. jejuni* is regulated by multi-drug exporter genes (*cmeABC*), we next checked the transcriptional profile of *cmeA*, *cmeB*, and *cmeC* transporter genes (Figures S5A–S5C). The data presented in Figure 4D indicates a significant up-regulation of all three genes of T6SS+ve *C. jejuni* in the presence of prey compared with a condition when the prey was unavailable. However, no significant differences in expressions of *cmeABC* genes were observed for T6SS-ve *C. jejuni* in the presence or absence of bile salt. Hence, the up-regulation of *cmeABC* genes in T6SS+ve *C. jejuni* indicates an intrinsic mechanism to mitigate the enhanced accumulation of intracellular bile salt, which in our case could be due to a prey-driven activation of the T6SS apparatus. This observation agrees with the previous studies suggesting the key role of T4SS (Bidlack and Silverman, 2004) and T6SS (Lertpiriyapong et al., 2012) as an open secretion system of bacteria in bile salt influx. No significant change was observed in *cmeABC* expressions among the T6SS+ve and T6SS-ve isolates in the absence of prey (Figure 4D), indicating that the CmeABC system behaves similarly for both isolates. This may eliminate the possibility of significant functional differences in *cme* genes.

Since oxidative stress induced by intracellular bile salt is known to have DNA-damaging activity (Prieto et al., 2006; Negretti et al., 2017), we further confirmed bile salt-induced DNA degradation in T6SS+ve *C. jejuni* in the presence of prey, but the DNA remained intact in the absence of its prey (Figure 4E). On the other hand, the DNA was unaffected in T6SS-ve *C. jejuni* under bile salt stress irrespective of prey's presence or absence (Figure S5D). However, in the absence of bile salt, the DNA smear was not observed when T6SS+ve *C. jejuni* was co-cultured with its prey; this excludes the possibility of T6SS-mediated DNA

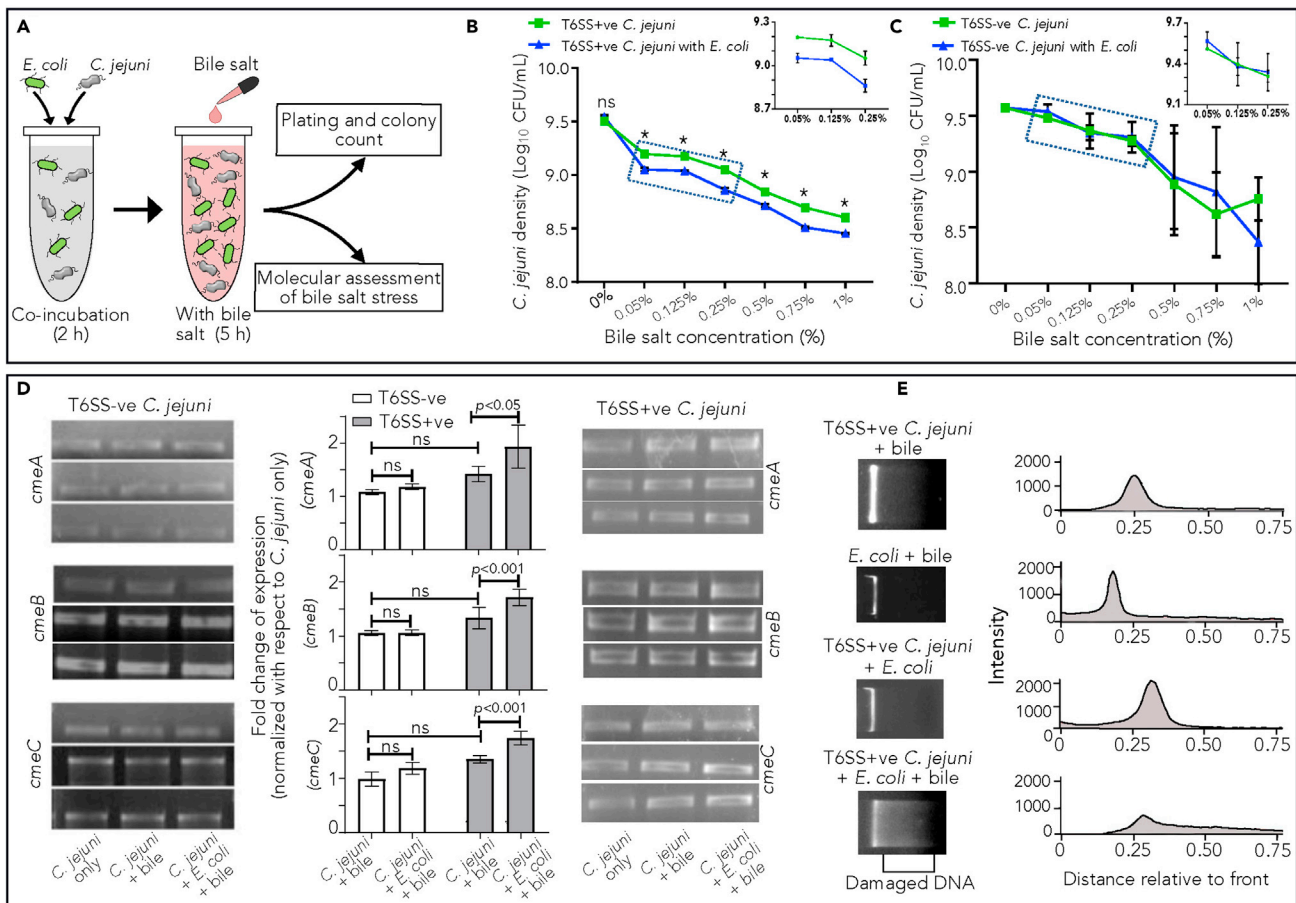


Figure 4. Effect of bile salt stress on T6SS-mediated predation

(A) Schematic of the experimental scheme to assess *C. jejuni* predation with bile salt.

(B and C) Densities of T6SS+ve (B) and T6SS-ve *C. jejuni* (C) at different bile salt concentrations, both in the absence and presence of prey ($n = 6$). Insets: Data inside the marked boxes are zoomed to highlight the decline in T6SS+ve *C. jejuni* population in the presence of prey, but this reduction was not observed for T6SS-ve *C. jejuni*.

(D) Expression of *Campylobacter* multidrug efflux genes (*cmeABC*) in T6SS+ve and T6SS-ve *C. jejuni* in the presence of bile salt (0.1%). Representative gel images of *cmeA*, *cmeB*, and *cmeC* genes are shown, from which relative fold changes over control (*C. jejuni* in the absence of bile salt) were quantified ($n = 8$). Data showed transcriptional up-regulation of all three genes in T6SS+ve *C. jejuni* when prey is present, but this was not seen for T6SS-ve *C. jejuni*.

(E) Gel images of DNA isolated from T6SS+ve *C. jejuni* (and corresponding intensity profiles) showed marked smear formation in the presence of prey and bile salt, indicating DNA damage (bottom). In B–E, initial counts of *E. coli* and *C. jejuni* were 6×10^7 CFU/mL and 3×10^8 CFU/mL, respectively. Error bars represent standard deviation (mean \pm SD).

damage of *E. coli*. Hence the observed DNA smearing may correspond to the direct effect of a high-level accumulation of bile salt in *C. jejuni*. To validate this further, we repeated the DNA smear assay and the transcriptional analysis of *cmeABC* genes with a T6SS-ve control strain, NCTC 11168, which does not contain the whole T6SS gene cluster (Serichantalergs et al., 2020). With this T6SS-ve control, we again reconfirm the “null” results found with our T6SS-ve isolate (Figures S5B–S5D), signifying that the absence of a functional T6SS is critical for bile salt tolerance.

Moreover, in the presence of bile salt, reactive oxygen species (ROS) may be produced, resulting in DNA fragmentation and DNA lesion, as reported previously (Negretti et al., 2017). To validate this, we quantified and visualized (by epifluorescence microscopy) the total ROS generation in *C. jejuni* in the presence or absence of bile salt and prey (see Figures S5E–S5H). Consistent with our DNA smear assay, we found that the presence of bile salt led to a higher amount of ROS in the T6SS+ve *C. jejuni* when the prey is present (Figures S5E and S5F). In contrast, the amount of total ROS in T6SS-ve isolates did not significantly change irrespective of the presence or absence of the prey (Figures S5G and S5H). Together, we propose

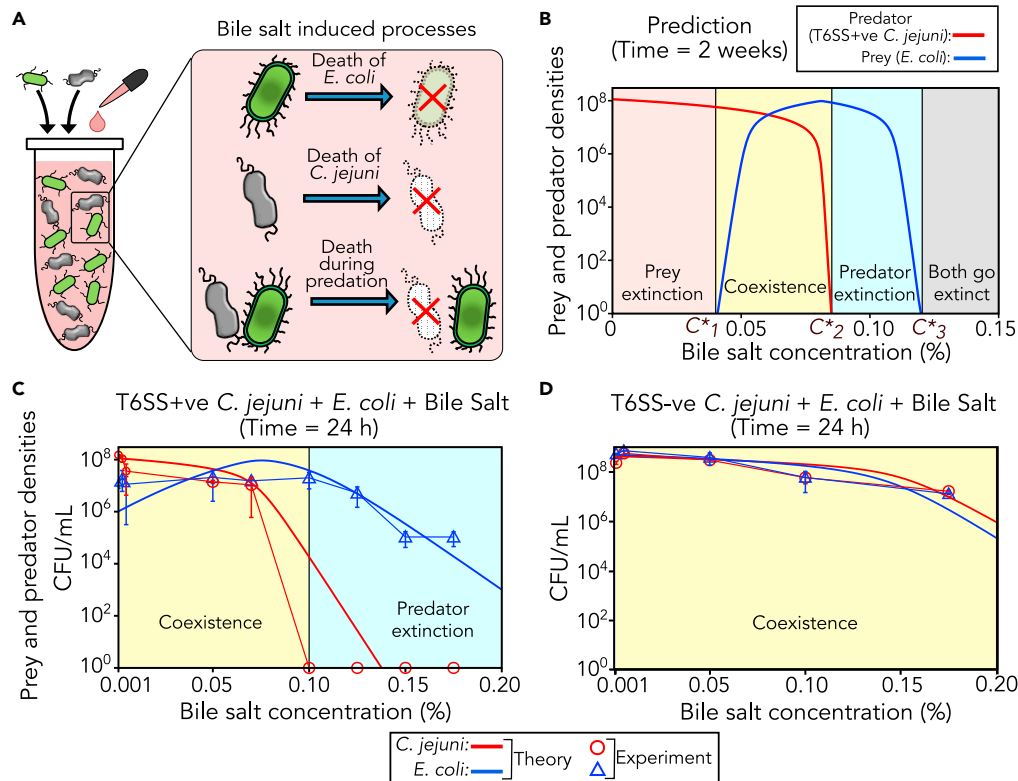


Figure 5. The cost of predation under stress dictates predator dominance versus extinction

(A) Schematic showing bile salt-induced death processes assumed to extend the predator-prey model under stress (see Equations 3 and 4).

(B) Model prediction of predator and prey densities in the steady state (i.e., at a large time) showing four possible outcomes when bile salt concentration is varied: extinction of prey, predator-prey coexistence, extinction of predator, and extinction of both. Boundaries between these regimes are marked, representing corresponding threshold concentrations (c^*_1 , c^*_2 , and c^*_3).

(C and D) Theoretical predictions (solutions of Equations 3 and 4) and measured densities of either T6SS+ve *C. jejuni* (C) or T6SS-ve *C. jejuni* (D) co-incubated with *E. coli* at different concentrations of bile salt for 24 h. Initial densities of *E. coli* and *C. jejuni* were 6×10^7 CFU/mL and 3×10^6 CFU/mL, respectively. Model parameters (for T6SS+ve *C. jejuni*): $r_p = 1.0/h$, $r_N = 0.4/h$, $K_p = 1.3 \times 10^8$ CFU/mL, $K_N = 3.7 \times 10^8$ CFU/mL, $\alpha = 7 \times 10^{-9}/h/(CFU/mL)$, $\beta_p = 11.0/(h \cdot conc.)$, $\beta_N = 5.0/(h \cdot conc.)$, and $\beta_{int} = 1.0 \times 10^{-9}/(h \cdot conc.)/(CFU/mL)$. We took $\alpha = \beta_{int} = 0$ for T6SS-ve *C. jejuni* as we expect no T6SS-dependent predation (see Table S2 and supplement information for details of parameter estimation). Of note, the T6SS-ve *C. jejuni* does not go extinct within the experimental range of the bile salt concentration. Error bars represent standard deviation (mean \pm SD).

(Also, see Figure S6L.)

that T6SS-mediated predation reduces the self-survival ability of *C. jejuni* under bile salt stress. This feature may advocate a cost of predation at the population level.

Model and data show predator extinction above a critical bile salt concentration

Having predation costs at the population level may lead to diverse ecological outcomes in terms of predator dominance. To explore this possibility, we extended the previously described model by including stress-induced death processes as below (see Figure 5A):

$$\frac{dP}{dt} = r_p P \left(1 - \frac{P}{K_p} \right) - \beta_p c P - \beta_{int} c N P \quad (\text{Equation 3})$$

$$\frac{dN}{dt} = r_N N \left(1 - \frac{N}{K_N} \right) - \alpha N P - \beta_N c N \quad (\text{Equation 4})$$

In the presence of bile salt, the predator and prey can die individually owing to its antimicrobial activity (described by $\beta_P cP$ and $\beta_N cN$, respectively in Equations 3 and 4). These deaths occur with rates $\beta_P c$ (for predators) and $\beta_N c$ (for preys), which are assumed proportional to the bile salt concentration, c . In addition, predators can die during the act of predation owing to stress-induced predation costs ($\beta_{int} c NP$), whose rate is $\beta_{int} c$.

We next obtained the parameter values of β_P and β_N from experiments with either T6SS+ve *C. jejuni* or *E. coli*, separately in bile salt solutions (Figures S6A–S6C, Table S3). Interestingly, T6SS+ve *C. jejuni* was found slightly less tolerant than *E. coli* with the bile salt ($\beta_P > \beta_N$). With a reasonable choice of β_{int} ($\beta_{int} = 1.0 \times 10^{-9}/h$, which is comparable, but less than α), our model predicts distinct ecological outcomes in the steady state (see Figure 5B). At very low concentrations of bile salt ($c < c_1^*$), the predation cost is not high, and hence predators can drive the prey extinct, whereas at intermediate concentrations ($c_1^* < c < c_2^*$) predators and prey coexist. The predation cost increases with the bile salt concentration, and when the concentration is above a threshold ($c > c_2^*$), predators themselves go extinct but preys stay alive. If the concentration is too high ($c > c_3^*$), as expected, both become extinct. The threshold concentrations separating these regimes (c_1^* , c_2^* , and c_3^*) were obtained analytically (see Figure S6 and STAR Methods for a detailed mathematical analysis).

Our model indicates that the steady state appears very late (roughly 2 weeks), and hence it is challenging to observe in experiments. We instead co-cultured T6SS+ve *C. jejuni* and *E. coli* in the presence of bile salt for 24 h to test our model prediction. Even at this short time, we found predator extinction beyond a critical concentration of bile salt and predator-prey coexistence below that level, consistent with our prediction (see Figure 5C). Of note, this threshold concentration obtained from the model is $c_2^* = 0.08\%$, and it is 0.1% in experiments after 24-h co-incubation. In contrast, predator extinction was not observed for T6SS-ve *C. jejuni* co-cultured with *E. coli*, and these data also agreed with the model by using $\alpha = \beta_{int} = 0$ (Figure 5D). Together, the proposed predation cost may determine predator dominance versus extinction during microbial interactions involving T6SS functionality.

Anti-predator host defense against *C. jejuni* under bile salt stress

To see whether the observed predation cost under stress can benefit the host against *C. jejuni* infection, we next challenged human intestinal epithelial cells (INT407) with T6SS+ve *C. jejuni* under four different environmental conditions (see schematic in Figure 6A). On the one hand, cells were infected with *C. jejuni* in the presence of bile salt solution. On the other hand, cells were co-incubated with *C. jejuni* and its prey (*E. coli*) under bile salt stress. The bile salt concentration was chosen to be 0.06%, based on the observed prey-predator coexistence (Figure 5C). Cells infected with only *C. jejuni* served as control.

Representative images of *C. jejuni* (stained with DAPI) invasion into live cells are shown in Figure 6B (also Figure S7). Cells incubated with *C. jejuni* showed significantly higher fluorescence intensity than the cells treated with *C. jejuni* and *E. coli* in the presence of bile salt, suggesting that fewer *C. jejuni* are available for cell invasion. Analysis of mean fluorescence intensity (MFI) also indicates little or no invasion into human INT407 cells in the presence of *E. coli* and bile salt (Figure 6C). This observation was further confirmed by the differential count of intracellular bacteria present in human INT407 cells (Figure 6D). The comparative abundance of *C. jejuni* invaded into cells may indicate that T6SS-mediated predation of *E. coli* facilitates self-killing of *C. jejuni* under bile salt stress. Therefore, the bile salt stress and high prey density effectively can protect host cells from T6SS-dependent cell cytotoxicity.

DISCUSSION

As contact-dependent secretion machinery, the T6SS aids in host colonization, niche dominance, and evasion of host defense for a range of gut pathogens (Watkins and Unnikrishnan, 2020; Hornung et al., 2018; Sana et al., 2017; Lin et al., 2019). Although *C. jejuni* possesses T6SS as a key toxin effector system (Noreen et al., 2018), unlike other bacteria, it lacks many classical virulence factors. Of note, *C. jejuni* maintains a single T6SS gene cluster with only one *hcp* gene in the locus to target other bacterial species (Noreen et al., 2018; Bleumink-Pluym et al., 2013; Russell et al., 2011). Analogous to T6SS, bacterial Cytolethal Distending Toxin (CDT) is another membrane-associated protein complex involved in host pathogenesis (Pickett et al., 1996; Young et al., 2007; Lara-Tejero and Galán, 2002). However, CDT exclusively binds to eukaryotic cells via cholesterol-rich microdomains on the cytoplasmic membrane (Gelfanova et al., 1999; Jinadasa et al., 2011); hence, CDT-mediated killing of other bacteria by *C. jejuni* is highly unlikely.

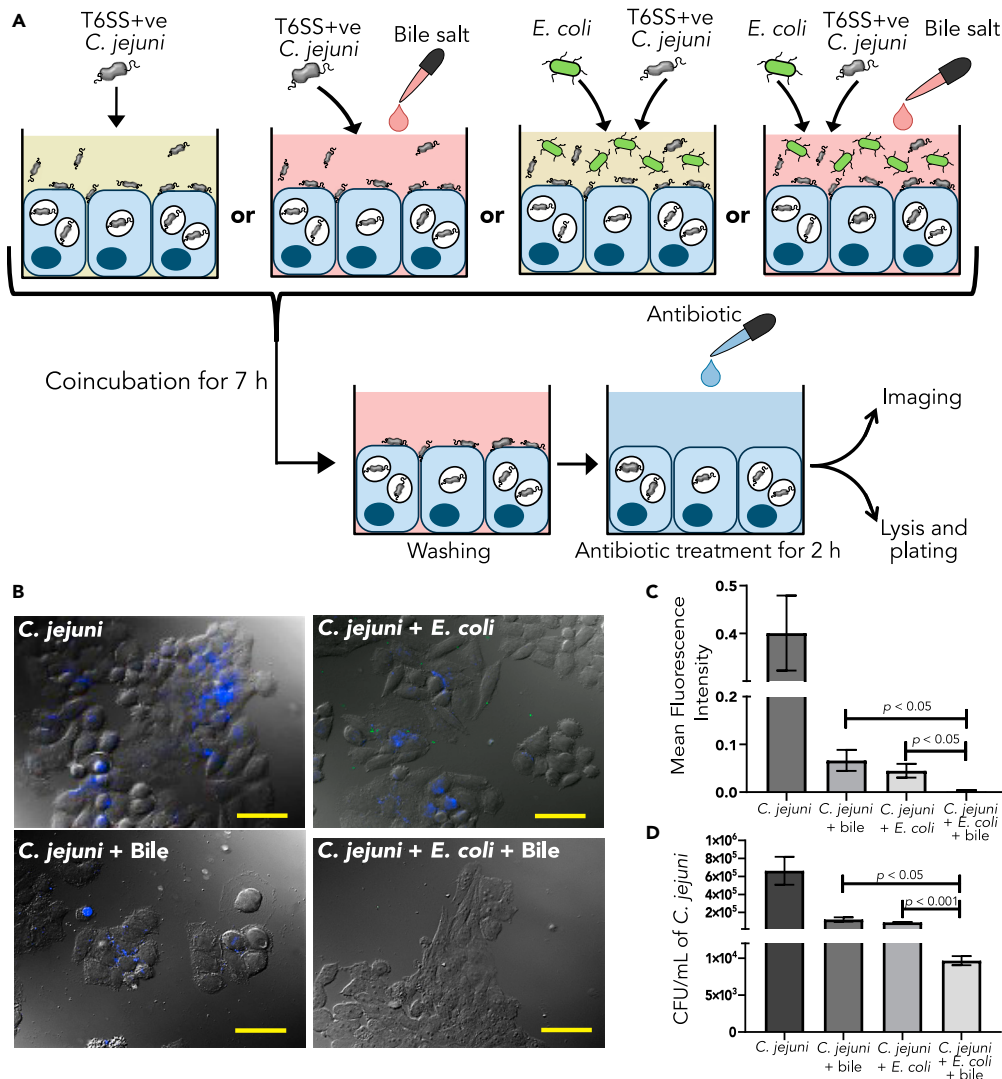


Figure 6. Bile salt-induced predation cost can reduce *C. jejuni* invasion of human intestinal epithelial cells

(A) Schematic of an experimental procedure to assess the ability of *C. jejuni* invasion in the presence of prey and bile salt solution. Confluent monolayers of human INT407 cells were co-incubated with T6SS+ve *C. jejuni* and *E. coli* in the presence of 0.06% bile salt solution for 7 h. Next, cells were washed to remove the extracellular bacteria and residual bile salt present in the medium. Furthermore, adhered bacteria were killed by antibiotic (gentamicin) treatment for 2 h. Finally, washed cells were either processed for imaging or lysed to count the intracellular *C. jejuni*. Initial counts of *C. jejuni* and *E. coli* were 4×10^6 CFU/mL and 8×10^7 CFU/mL, respectively. Infection of cells was performed at 300:1 MOI.

(B) Representative images of *C. jejuni* (stained with DAPI) invasion of INT407 cells (Scale bar: 50 μ m).

(C) Cells incubated with only *C. jejuni* showed significantly higher mean fluorescence intensity (MFI) than the cells treated with *C. jejuni* in the presence of *E. coli* and bile salt, suggesting almost none or few *C. jejuni* available for the cell invasion ($n = 6$).

(D) The count (CFU/mL) of invaded *C. jejuni* released from the lysed INT407 cells. Data suggest a significant reduction of cellular invasion by *C. jejuni* in the presence of *E. coli* and bile salt. Error bars represent standard deviation (mean \pm SD) ($n = 6$).

Although the T6SS can confer fitness advantage over other competing microbes within the same niche (Dörr and Bloesch, 2018), the question remains whether the functionality of T6SS entails any cost during bacterial predation. A recent study showed that T6SS-dependent predation could promote DNA uptake from the target cells, resulting in delayed cell division of the predator population (Lin et al., 2019). Complementarily, we showed that a functional T6SS might exhibit a distinct disadvantage in a harsh gut environmental condition where we used bile salt (an integral component of the gut) as natural stress. In the

presence of prey, we observed a significant decline in the T6SS+ve *C. jejuni* population under the bile salt stress, whereas no such effect was seen in T6SS-ve *C. jejuni* (Figures 4B, 4C, and S6L). We further reproduced this differential stress response in a series of T6SS+ve and T6SS-ve *C. jejuni* isolates (Figure S4), signifying a generic phenotypic difference among *C. jejuni* strains, where bacterial usage of the T6SS apparatus may emerge as a predation cost. However, the adaptability of gut microbes toward environmental stress (such as bile salt) is a complex question.

The multi-drug-exporter genes (*cmeABC*) remain the exclusive transporter system that regulates bile salt tolerance to *C. jejuni*. Here, we showed up-regulation of *cmeABC* genes solely in T6SS+ve isolates under the bile salt stress when the prey is available (Figures 4D and S5A). Enhanced expression of *cmeABC* genes could be evidence from higher accumulation of intracellular bile salt, which advocates the role of T6SS as an open secretion channel to facilitate bile salt influx (Bidlack and Silverman, 2004; Lertpiriyapong et al., 2012). This proposal is in line with a recent study that suggests the function of T6SS as a bidirectional effector secretion system, given its ability to contract in opposite directions (Szwedziak and Pilhofer, 2019). In addition, we observed a direct correlation among up-regulation of *cmeABC* genes, enhanced ROS generation, and elevated DNA damage leading to cell death (Figures 4D, 4E, and S5).

Taken together, under bile salt stress, T6SS harboring predators may die during the very act of predation (Lertpiriyapong et al., 2012). To assess how this predation cost impacts predator-prey population dynamics in changing bile salt concentration, we developed a mathematical model. We found that diverse ecological outcomes, such as predator-prey coexistence and prey or predator extinction, emerge in a concentration-dependent manner. Consistent with our model, we found prey-predator coexistence below a critical bile salt concentration (0.1%), whereas predators go extinct above this level (Figure 5C). This addresses an interesting question: can the T6SS harboring bacteria often win during a microbial competition by killing other T6SS-ve prey species? In contrast, T6SS+ve *C. jejuni* exhibits commensalism in the chicken gut, where prey-predators coexist. The bile salt concentration in the chicken cecum was reported to be ~0.009%, which is well below the observed critical level (Lin et al., 2003). On the other hand, the concentration of bile salts in the human small intestine ranges from 0.2% to 2%, which is too high to expect predator-prey coexistence (Kristoffersen et al., 2007). This may explain the selective predominance of T6SS+ve *C. jejuni* in chickens as a natural commensal (Humphrey et al., 2014; Newell and Fearnley, 2003). Nevertheless, the *in vivo* emergence of predator-prey coexistence can also depend on the spatially heterogeneous gut landscape that can produce refuge patches for the prey, similar to the models of phage-bacteria interactions (Heilmann et al., 2012).

The cost of T6SS-mediated predation under specific stress can further have evolutionary implications. A recent study suggests that a random firing of T6SS machinery can have a more selective advantage to win the microbial competition than a “tit-for-tat” mechanism, by which the T6SS-harboring bacterium counterattacks only if it is under attack by similar T6SS apparatus (Smith et al., 2020). However, our findings indicate that a random firing of T6SS, if it takes place, can be “costlier” under bile salt stress since this may increase the chance of bile salt influx into the cell. Given the cost of expressing the T6SS under stress, T6SS-ve bacteria may also exhibit “cheating” behavior if they “lure” the T6SS+ve bacteria as their prey. This may have important eco-evolutionary consequences during the intraspecies competition (Sanchez and Gore, 2013; Smith and Schuster, 2019).

Moreover, it was shown that exposure to short and moderate sodium chloride stress helps bacterial survival during a later period of stress, indicating a “memory-like” effect (Mathis and Ackermann, 2016). Whether such an effect emerges in our case via interaction of T6SS with the environment is an interesting open question. Another corollary of our study is that the preys’ cell-division delay could be a “cope-up” mechanism against the predator stress (Figures 2B and 2C). Thus, it could be interesting to explore if a phenotypic variation in lag time can benefit prey in evasion of predator stress (Moreno-Gómez et al., 2020).

Finally, we explored the translational potential of bile salt-induced predation cost of *C. jejuni* in an *in vitro* setup using human intestinal epithelial cells (INT407). We showed a significant reduction (~10-fold) in the intracellular count of *C. jejuni* when co-cultured with its prey and bile salt. Therefore, the bile salt stress and prey’s availability effectively protect host cells from T6SS-mediated cell cytotoxicity. Although this host defense strategy seems to work *in vitro*, a systematic analysis of host immune regulatory factors in other cell types is required. Nevertheless, our proof-of-principle experiments with human cells advocate the concomitant use of non-pathogenic prey bacteria and bile salt as a potential antimicrobial alternative to mitigate intestinal colonization of gut pathogens (Nag et al., 2018).

Limitations of the study

The present study showed that T6SS+ve isolates of *C. jejuni* are more susceptible to bile salt stress during predation than T6SS-ve isolates (Figures 4B, 4C, and S4). Hence, we proposed that the T6SS+ve *C. jejuni* exhibits a “cost of T6SS-dependent predation” as an ecological outcome. Although a series of wild isolates were extensively characterized based on the essential genes of T6SS, we think that *loss-of-function mutations* in the isogenic background (deletion mutant of T6SS) could provide more insights to support the proposed mechanism. Moreover, a better understanding of T6SS functionality in the transportation of biological macromolecules requires real-time tracking.

STAR★METHODS

Detailed methods are provided in the online version of this paper and include the following:

- KEY RESOURCES TABLE
- RESOURCE AVAILABILITY
 - Lead contact
 - Materials availability
 - Data and code availability
- EXPERIMENTAL MODEL AND SUBJECT DETAILS
 - Bacteria
 - Cell line
 - Bacterial vectors
- METHOD DETAILS
 - Genotypic profiling and functional characterization of *C. jejuni* isolated from chickens
 - Generation of GFP expressing prey bacteria (*E. coli*)
 - Experimental set up for studying prey-predator interaction
 - Differential cell invasion ability of *C. jejuni*
 - Mathematical analysis
 - Linear stability analysis
- QUANTIFICATION AND STATISTICAL ANALYSIS
 - Image analysis

SUPPLEMENTAL INFORMATION

Supplemental information can be found online at <https://doi.org/10.1016/j.isci.2021.103507>.

ACKNOWLEDGMENTS

S.G. and A.K. thank UGC, MoE, Govt. of India, for fellowship support. A.I.M. and D.D. acknowledge IISER Kolkata for experimental facilities. Computational facilities were supported by grants from DBT Ramalingaswami Fellowship, India and SERB (SRG), DST, India to D.D. We thankfully acknowledge Dr. P. P. Datta for providing *pTurbo*-GFP-B plasmid and Dr. R. Das for helpful discussion.

AUTHOR CONTRIBUTIONS

S.G. performed all experiments. S.R. developed the mathematical model and performed data analysis. A.K. assisted in phenotypic characterization of the test strains and A.C. helped in plate counting and data analysis. D.D. and A.I.M. conceived the study and wrote the manuscript with support from S.G., S.R., and A.C. Quantitative/theoretical works were supervised by D.D. and experimental works were supervised by A.I.M.

DECLARATION OF INTERESTS

The authors declare no competing interests.

Received: July 14, 2021

Revised: October 21, 2021

Accepted: November 22, 2021

Published: December 17, 2021

REFERENCES

- Abby, S.S., Cury, J., Guglielmini, J., Néron, B., Touchon, M., and Rocha, E.P.C. (2016). Identification of protein secretion systems in bacterial genomes. *Sci. Rep.* 6, 23080. <https://doi.org/10.1038/srep23080>.
- Awad, W.A., Hess, C., and Hess, M. (2018). Rethinking the chicken–*Campylobacter jejuni* interaction: a review. *Avian Pathol.* 47, 352–363. <https://doi.org/10.1080/03079457.2018.1475724>.
- Basler, M., Pilhofer, M., Henderson, G.P., Jensen, G.J., and Mekalanos, J.J. (2012). Type VI secretion requires a dynamic contractile phage tail-like structure. *Nature* 483, 182–186. <https://doi.org/10.1038/nature10846>.
- Basler, M., Ho, B.T., and Mekalanos, J.J. (2013). Tit-for-tat: type VI secretion system counterattack during bacterial cell-cell interactions. *Cell* 152, 884–894. <https://doi.org/10.1016/j.cell.2013.01.042>.
- Begley, M., Gahan, C.G.M., and Hill, C. (2005). The interaction between bacteria and bile. *FEMS Microbiol. Rev.* 29, 625–651. <https://doi.org/10.1016/j.femsrev.2004.09.003>.
- Beski, S.S.M., Swick, R.A., and Iji, P.A. (2015). Specialized protein products in broiler chicken nutrition: a review. *Anim. Nutr.* 1, 47–53. <https://doi.org/10.1016/j.aninu.2015.05.005>.
- Bhattacharyya, S., Purkait, K., and Mukherjee, A. (2017). Ruthenium(II) p-cymene complexes of a benzimidazole-based ligand capable of VEGFR2 inhibition: hydrolysis, reactivity and cytotoxicity studies. *Dalton Trans.* 46, 8539–8554. <https://doi.org/10.1039/C7DT00938K>.
- Bidlack, J.E., and Silverman, P.M. (2004). An active type IV secretion system encoded by the F plasmid sensitizes *Escherichia coli* to bile salts. *J. Bacteriol.* 186, 5202–5209. <https://doi.org/10.1128/JB.186.16.5202-5209.2004>.
- Bleumink-Pluym, N.M.C., Alphen, L.B.van, Bouwman, L.I., Wösten, M.M.S.M., and Putten, J.P.M.van (2013). Identification of a functional type VI secretion system in *Campylobacter jejuni* conferring capsule polysaccharide sensitive cytotoxicity. *PLOS Pathog.* 9, e1003393. <https://doi.org/10.1371/journal.ppat.1003393>.
- Chen, C., Yang, X., and Shen, X. (2019). Confirmed and potential roles of bacterial T6SSs in the intestinal ecosystem. *Front. Microbiol.* 10, 1484. <https://doi.org/10.3389/fmicb.2019.01484>.
- Cianfanelli, F.R., Monlezun, L., and Coulthurst, S.J. (2016). Aim, load, fire: the type VI secretion system, a bacterial nanoweapon. *Trends Microbiol.* 24, 51–62. <https://doi.org/10.1016/j.tim.2015.10.005>.
- David, L.A., Materna, A.C., Friedman, J., Campos-Baptista, M.I., Blackburn, M.C., Perrotta, A., Erdman, S.E., and Alm, E.J. (2014). Host lifestyle affects human microbiota on daily timescales. *Genome Biol.* 15, R89. <https://doi.org/10.1186/gb-2014-15-7-r89>.
- Desvaux, M., and Hébraud, M. (2006). The protein secretion systems in *Listeria*: inside out bacterial virulence. *FEMS Microbiol. Rev.* 30, 774–805. <https://doi.org/10.1111/j.1574-6976.2006.00035.x>.
- Dörr, N.C.D., and Blokesch, M. (2018). Bacterial type VI secretion system facilitates niche domination. *PNAS* 115, 8855–8857. <https://doi.org/10.1073/pnas.1812776115>.
- Fast, D., Kostiuk, B., Foley, E., and Pukatzki, S. (2018). Commensal pathogen competition impacts host viability. *Proc. Natl. Acad. Sci. U S A.* 115, 7099–7104. <https://doi.org/10.1073/pnas.1802165115>.
- Gelfanova, V., Hansen, E.J., and Spinola, S.M. (1999). Cytolethal distending toxin of *Haemophilus ducreyi* induces apoptotic death of Jurkat T cells. *Infect. Immun.* 67, 6394–6402. <https://doi.org/10.1128/IAI.67.12.6394-6402.1999>.
- Green, E.R., and Mecsas, J. (2016). Bacterial secretion systems – an overview. *Microbiol. Spectr.* 4, 4-1. <https://doi.org/10.1128/microbiolspec.VMBF-0012-2015>.
- Grinnage-Pulley, T., Mu, Y., Dai, L., and Zhang, Q. (2016). Dual repression of the multidrug efflux pump CmeABC by CosR and CmeR in *Campylobacter jejuni*. *Front. Microbiol.* 7, 1097. <https://doi.org/10.3389/fmicb.2016.01097>.
- Heilmann, S., Sneppen, K., and Krishna, S. (2012). Coexistence of phage and bacteria on the boundary of self-organized refuges. *PNAS* 109, 12828–12833. <https://doi.org/10.1073/pnas.1200771109>.
- Hersch, S.J., Manera, K., and Dong, T.G. (2020). Defending against the type six secretion system: beyond immunity genes. *Cell Rep.* 33, 108259. <https://doi.org/10.1016/j.celrep.2020.108259>.
- Hornung, B., Martins dos Santos, V.A.P., Smidt, H., and Schaap, P.J. (2018). Studying microbial functionality within the gut ecosystem by systems biology. *Genes Nutr.* 13, 5. <https://doi.org/10.1186/s12263-018-0594-6>.
- Humphrey, S., Chaloner, G., Kemmett, K., Davidson, N., Williams, N., Kipar, A., Humphrey, T., and Wigley, P. (2014). *Campylobacter jejuni* not merely a commensal in commercial broiler chickens and affects bird welfare. *mBio* 5, e01364–14. <https://doi.org/10.1128/mBio.01364-14>.
- Jinadasa, R.N., Bloom, S.E., Weiss, R.S., and Duhamel, G.E. (2011). Cytolethal distending toxin: a conserved bacterial genotoxin that blocks cell cycle progression, leading to apoptosis of a broad range of mammalian cell lineages. *Microbiology (Reading)* 157, 1851–1875. <https://doi.org/10.1099/mic.0.049536-0>.
- Kristoffersen, S.M., Ravnum, S., Tourasse, N.J., Økstad, O.A., Kolstø, A.-B., and Davies, W. (2007). Low concentrations of bile salts induce stress responses and reduce motility in *Bacillus cereus* ATCC 14570. *J. Bacteriol.* 189, 5302–5313. <https://doi.org/10.1128/JB.00239-07>.
- Lara-Tejero, M., and Galán, J.E. (2002). Cytolethal distending toxin: limited damage as a strategy to modulate cellular functions. *Trends Microbiol.* 10, 147–152. [https://doi.org/10.1016/s0966-842x\(02\)02316-8](https://doi.org/10.1016/s0966-842x(02)02316-8).
- Lee, A.W.C., Li, J.-H., Shi, W., Li, A., Ng, E., Liu, T.-J., Klamut, H.J., and Liu, F.-F. (2003). p16 gene therapy: a potentially efficacious modality for nasopharyngeal carcinoma. *Mol. Cancer Ther.* 2, 961–969.
- Lertpiriyapong, K., Gamazon, E.R., Feng, Y., Park, D.S., Pang, J., Botka, G., Graffam, M.E., Ge, Z., and Fox, J.G. (2012). *Campylobacter jejuni* type VI secretion system: roles in adaptation to deoxycholic acid, host cell adherence, invasion, and in vivo colonization. *PLOS ONE* 7, e42842. <https://doi.org/10.1371/journal.pone.0042842>.
- Lin, J., Michel, L.O., and Zhang, Q. (2002). CmeABC functions as a multidrug efflux system in *Campylobacter jejuni*. *Antimicrob. Agents Chemother.* 46, 2124–2131. <https://doi.org/10.1128/AAC.46.7.2124-2131.2002>.
- Lin, J., Sahin, O., Michel, L.O., and Zhang, Q. (2003). Critical role of multidrug efflux pump CmeABC in bile resistance and in vivo colonization of *Campylobacter jejuni*. *Infect. Immun.* 71, 4250–4259. <https://doi.org/10.1128/IAI.71.8.4250-4259.2003>.
- Lin, L., Ringel, P.D., Vettiger, A., Dürr, L., and Basler, M. (2019). DNA uptake upon T6SS-dependent prey cell lysis induces SOS response and reduces fitness of *Acinetobacter baylyi*. *Cell Rep.* 29, 1633–1644.e4. <https://doi.org/10.1016/j.celrep.2019.09.083>.
- Margolin, W. (2005). FtsZ and the division of prokaryotic cells and organelles. *Nat. Rev. Mol. Cell Biol.* 6, 862–871. <https://doi.org/10.1038/nrm1745>.
- Mathis, R., and Ackermann, M. (2016). Response of single bacterial cells to stress gives rise to complex history dependence at the population level. *PNAS* 113, 4224–4229. <https://doi.org/10.1073/pnas.1511509113>.
- Moreno-Gámez, S., Kiviet, D.J., Vulin, C., Schlegel, S., Schlegel, K., Doorn, G.S.van, and Ackermann, M. (2020). Wide lag time distributions break a trade-off between reproduction and survival in bacteria. *PNAS* 117, 18729–18736. <https://doi.org/10.1073/pnas.2003331117>.
- Mougous, J.D., Cuff, M.E., Raunser, S., Shen, A., Zhou, M., Gifford, C.A., Goodman, A.L., Joachimiak, G., Ordoñez, C.L., Lory, S., et al. (2006). A virulence locus of *Pseudomonas aeruginosa* encodes a protein secretion apparatus. *Science* 312, 1526–1530. <https://doi.org/10.1126/science.1128393>.
- Nag, D., Breen, P., Raychaudhuri, S., and Withey, J.H. (2018). Glucose metabolism by *Escherichia coli* inhibits *Vibrio cholerae* intestinal colonization of zebrafish. *Infect. Immun.* 86, e00486-18. <https://doi.org/10.1128/IAI.00486-18>.
- Negretti, N.M., Gourley, C.R., Clair, G., Adkins, J.N., and Konkel, M.E. (2017). The food-borne pathogen *Campylobacter jejuni* responds to the bile salt deoxycholate with countermeasures to reactive oxygen species. *Sci. Rep.* 7, 15455. <https://doi.org/10.1038/s41598-017-15379-5>.
- Newell, D.G., and Fearnley, C. (2003). Sources of *Campylobacter* colonization in broiler chickens. *Appl. Environ. Microbiol.* 69, 4343–4351. <https://doi.org/10.1128/aem.69.8.4343-4351.2003>.

- Noreen, Z., Jobichen, C., Abbasi, R., Seetharaman, J., Sivaraman, J., and Bokhari, H. (2018). Structural basis for the pathogenesis of *Campylobacter jejuni* Hcp1, a structural and effector protein of the Type VI Secretion System. *FEBS J.* 285, 4060–4070. <https://doi.org/10.1111/febs.14650>.
- Pickett, C.L., Pesci, E.C., Cottle, D.L., Russell, G., Erdem, A.N., and Zeytin, H. (1996). Prevalence of cytolethal distending toxin production in *Campylobacter jejuni* and relatedness of *Campylobacter* sp. cdtB gene. *Infect. Immun.* 64, 2070–2078. <https://doi.org/10.1128/iai.64.6.2070-2078.1996>.
- Prieto, A.I., Ramos-Morales, F., and Casadesús, J. (2006). Repair of DNA damage induced by bile salts in *Salmonella enterica*. *Genetics* 174, 575–584. <https://doi.org/10.1534/genetics.106.060889>.
- Priya, S., and Blekman, R. (2019). Population dynamics of the human gut microbiome: change is the only constant. *Genome Biol.* 20, 150. <https://doi.org/10.1186/s13059-019-1775-3>.
- Russell, A.B., Hood, R.D., Bui, N.K., LeRoux, M., Vollmer, W., and Mougous, J.D. (2011). Type VI secretion delivers bacteriolytic effectors to target cells. *Nature* 475, 343–347. <https://doi.org/10.1038/nature10244>.
- Sana, T.G., Lugo, K.A., and Monack, D.M. (2017). T6SS: the bacterial “fight club” in the host gut. *Plos Pathog.* 13, e1006325. <https://doi.org/10.1371/journal.ppat.1006325>.
- Sanchez, A., and Gore, J. (2013). Feedback between population and evolutionary dynamics determines the fate of social microbial populations. *PLoS Biol.* 11, e1001547. <https://doi.org/10.1371/journal.pbio.1001547>.
- Schell, M.A., Ulrich, R.L., Ribot, W.J., Brueggemann, E.E., Hines, H.B., Chen, D., Lipscomb, L., Kim, H.S., Mrázek, J., Nierman, W.C., and Deshazer, D. (2007). Type VI secretion is a major virulence determinant in *Burkholderia mallei*. *Mol. Microbiol.* 64, 1466–1485. <https://doi.org/10.1111/j.1365-2958.2007.05734.x>.
- Schwarz, S., West, T.E., Boyer, F., Chiang, W.-C., Carl, M.A., Hood, R.D., Rohmer, L., Tolker-Nielsen, T., Skerrett, S.J., and Mougous, J.D. (2010). Burkholderia type VI secretion systems have distinct roles in eukaryotic and bacterial cell interactions. *PLoS Pathog.* 6, e1001068. <https://doi.org/10.1371/journal.ppat.1001068>.
- Serichantalergs, O., Wassanarungroj, P., Khemnu, N., Poly, F., Guerry, P., Bodhidatta, L., Crawford, J., and Swierczewski, B. (2020). Distribution of genes related to Type 6 secretion system and lipooligosaccharide that induced ganglioside mimicry among *Campylobacter jejuni* isolated from human diarrhea in Thailand. *Gut Pathog.* 12, 18. <https://doi.org/10.1186/s13099-020-00357-6>.
- Sha, J., Rosenzweig, J.A., Kozlova, E.V., Wang, S., Erova, T.E., Kirtley, M.L., van Lier, C.J., and Chopra, A.K. (2013). Evaluation of the roles played by Hcp and VgrG type 6 secretion system effectors in *Aeromonas hydrophila* SSU pathogenesis. *Microbiology* 159, 1120–1135. <https://doi.org/10.1099/mic.0.063495-0>.
- Singh, A., and Mallick, A.I. (2019). Role of putative virulence traits of *Campylobacter jejuni* in regulating differential host immune responses. *J. Microbiol.* 57, 298–309. <https://doi.org/10.1007/s12275-019-8165-0>.
- Singh, A., Nisaa, K., Bhattacharyya, S., and Mallick, A.I. (2019). Immunogenicity and protective efficacy of mucosal delivery of recombinant hcp of *Campylobacter jejuni* Type VI secretion system (T6SS) in chickens. *Mol. Immunol.* 111, 182–197. <https://doi.org/10.1016/j.molimm.2019.04.016>.
- Smith, P., and Schuster, M. (2019). Public goods and cheating in microbes. *Curr. Biol.* 29, R442–R447. <https://doi.org/10.1016/j.cub.2019.03.001>.
- Smith, W.P.J., Brodmann, M., Unterweger, D., Davit, Y., Comstock, L.E., Basler, M., and Foster, K.R. (2020). The evolution of tit-for-tat in bacteria via the type VI secretion system. *Nat. Commun.* 11, 5395. <https://doi.org/10.1038/s41467-020-19017-z>.
- Szwedziak, P., and Pilhofer, M. (2019). Bidirectional contraction of a type six secretion system. *Nat. Commun.* 10, 1565. <https://doi.org/10.1038/s41467-019-09603-1>.
- Varon, M., and Zeigler, B.P. (1978). Bacterial predator-prey interaction at low prey density. *Appl. Environ. Microbiol.* 36, 11–17.
- Wang, M., Luo, Z., Du, H., Xu, S., Ni, B., Zhang, H., Sheng, X., Xu, H., and Huang, X. (2011). Molecular characterization of a functional type VI secretion system in *Salmonella enterica* serovar Typhi. *Curr. Microbiol.* 63, 22–31. <https://doi.org/10.1007/s00284-011-9935-z>.
- Watkins, K., and Unnikrishnan, M. (2020). Chapter 9 - new strategies and targets for antibacterial discovery. In *Drug Discovery Targeting Drug-Resistant Bacteria*, P. Kesharwani, S. Chopra, and A. Dasgupta, eds. (Academic Press), pp. 249–272. <https://doi.org/10.1016/B978-0-12-818480-6.00009-6>.
- Williams, T., and Kelley, C. (2011). An Interactive Plotting Program 225. <http://gnuplot.info>.
- Wood, T.E., Aksoy, E., and Hachani, A. (2020). From welfare to warfare: the Arbitration of host-microbiota interplay by the type VI secretion system. *Front. Cell. Infect. Microbiol.* 10, 613. <https://doi.org/10.3389/fcimb.2020.587948>.
- Young, K.T., Davis, L.M., and DiRita, V.J. (2007). *Campylobacter jejuni*: molecular biology and pathogenesis. *Nat. Rev. Microbiol.* 5, 665–679. <https://doi.org/10.1038/nrmicro1718>.
- Yu, M., and Lai, E.-M. (2017). Warfare between host immunity and bacterial weapons. *Cell Host Microbe* 21, 3–4. <https://doi.org/10.1016/j.chom.2016.12.012>.

STAR★METHODS

KEY RESOURCES TABLE

REAGENT or RESOURCE	SOURCE	IDENTIFIER
Antibodies		
Goat anti-Rabbit IgG (HRP Conjugated)	BioBharati LifeScience Pvt Ltd, India	Cat# BB-SAB01C
Bacterial and virus strains		
<i>Campylobacter jejuni</i> (Strain: NCTC 11168)	BEI Resources, USA	Cat# NR-126
<i>E. coli</i> (DH5 α)	BioBharati LifeScience Pvt Ltd, India	Cat# BB-X0051
Chemicals, peptides, and recombinant proteins		
Blood Free <i>Campylobacter</i> Selectivity Agar Base Medium	HiMedia, India	Cat# M887
CAT Selective Supplement	HiMedia, India	Cat# FD 145
Muller-Hinton Broth	HiMedia, India	Cat# M391
Trichloro acetic acid	Merck	Cat# 1.94971.0521
X-gal	HiMedia, India	Cat# MB069
IPTG	BioBharati LifeScience Pvt Ltd, India	Cat# BB-C0010
Vecta-Sheild Mounting Media	Vector Laboratories, Inc., Burlingame, CA	Cat# H-1000-10
Glutaraldehyde	Merck	Cat# 8.20603.0521
TRizol® Reagent	Ambion (Life Technologies)	Cat# 15596026
Superscript Reverse Transcriptase Kit	BioBharati LifeScience Pvt Ltd, India	Cat# BB-E043
Bile salt mixture	HiMedia, India	Cat# RM009-100G
2',7'- Dichlorodihydrofluorescein diacetate	Thermo Fisher Scientific (Invitrogen)	Cat# D399
Dulbecco's Modified Eagle Medium (DMEM)	Gibco (Invitrogen)	Cat# 11995-065
FBS	Invitrogen	Cat# 10270106
Gentamicin	HiMedia, India	Cat# CMS461-1G
Triton X-100	Sigma-Aldrich	Cat# T8787-100ML
DAPI	USB Corporation	Cat# 14564 10M
Software and algorithms		
Zen	Carl ZEISS, Germany	https://www.zeiss.com/microscopy/int/products/microscope-software/zen-lite.html
ImageLab	Bio-Rad Laboratories, Inc.	https://www.bio-rad.com/en-in/product/image-lab-software?ID=KRE6P5E8Z
SoftMax® Pro Microplate Data Acquisition and analysis software	Molecular devices, LLC.	https://www.bioz.com.softmaxpro6.2.2.product
ImageJ	Rasband, W.S., ImageJ, U. S. National Institutes of Health, Bethesda, Maryland, USA	https://imagej.nih.gov/ij/ , 1997-2018
Graphpad Prism 8.0	GraphPad, USA	http://www.graphpad.com/
Inkscape, (Version 0.92.5)	Inkscape Project, 2020.	https://inkscape.org/
Gnuplot (version 5.2.8)	(Williams and Kelley, 2011)	http://www.gnuplot.info/
Mathematica	Wolfram Research, Inc.	https://www.wolfram.com/mathematica/

RESOURCE AVAILABILITY

Lead contact

Further information and requests for resources and reagents should be directed to and will be fulfilled by the lead contact, Dr. Amirul Islam Mallick (amallick@iiserkol.ac.in).

Materials availability

This study did not generate new unique reagents.

Data and code availability

- All data (such as population count, transcriptional analysis, and imaging data) are presented in the Figures. Data are also available upon reasonable request by contacting the lead contact.
- The model equations (Equations 1, 2, 3 and 4) were solved using Mathematica codes. All Mathematica codes are freely available at the following site: <https://github.com/raysou/Predator-prey-dynamics.git>. These codes can be used to generate theoretical curves presented in the study.

EXPERIMENTAL MODEL AND SUBJECT DETAILS

Bacteria

All of the *C. jejuni* strains were isolated locally except the standard strain (NCTC 11168). The standard *C. jejuni* strain (NCTC 11168; Genbank ID: AL111168.1) was obtained through the NIH Biodefense and Emerging Infections Research Repository, NIAID, NIH: *Campylobacter jejuni* subsp. *jejuni*, Strain NCTC 11168, NR-126. The *E. coli* (DH5 α) cells were obtained from BioBharati LifeScience Pvt Ltd, India.

Cell line

Human INT407 cells were obtained from NCCS, Pune, India. Cells were maintained at 37°C with 5% CO₂ in complete DMEM supplemented with 10% FBS (v/v), 100 IU/mL of penicillin and 100 mg/mL of streptomycin.

Bacterial vectors

We employed pTurboGFP-B plasmid into *E. coli* (DH5 α) cells for better visualization. This vector was provided by Dr. P. P. Datta.

METHOD DETAILS

Genotypic profiling and functional characterization of *C. jejuni* isolated from chickens

Isolation and identification of *C. jejuni*. To isolate *C. jejuni*, the cecal content of commercial broiler chickens was collected and processed (Singh and Mallick, 2019). Processed samples were plated onto a blood Free Campylobacter Selectivity Agar Base medium (HiMedia, India) supplemented with CAT selective supplement (cefoperazone 8 mg/L, amphotericin 10 mg/L, and teicoplanin 4 mg/L) (HiMedia, India) and incubated for 36-48 h at 42°C. Colonies were examined for characteristic morphological appearance followed by biochemical analysis including catalase, oxidase, and hippurate hydrolysis test. Further, selected colonies were checked for the presence of 16S rRNA and other major genes encoding virulence factors (GEVFs), including *hipO*, *cadF*, *ciaB* genes.

The standard *C. jejuni* strain (NCTC 11168; Genbank ID: AL111168.1) was obtained through the NIH Biodefense and Emerging Infections Research Repository, NIAID, NIH: *Campylobacter jejuni* subsp. *jejuni*, Strain NCTC 11168, NR-126.

Identification of T6SS+ve *C. jejuni*. Molecular identification of T6SS+ve *C. jejuni* among the isolates was confirmed through PCR using primers specific to *C. jejuni* T6SS such as *vasC*, *vasK*, *hcp*, *vasE* and *vasD* (see Table S1 for the genotypes of isolates and Table S2 for the list of primers).

Functional characterization of *C. jejuni* T6SS. To confirm the ability of T6SS+ve *C. jejuni* to secrete Hcp protein as a hallmark of functional T6SS, culture supernatant was collected when the OD reached 1.00 (A₆₀₀~1). Next, total proteins present in the supernatant were precipitated by 10% trichloroacetic acid (TCA) followed by washing with chilled acetone (centrifugation at 8000 xg for 20 mins. at 4°C). Finally, the washed pellet was re-suspended in PBS (pH~7.4) and subjected for immunoblotting and indirect ELISA using a polyclonal anti-Hcp antibody, raised in New Zealand White rabbit.

Generation of GFP expressing prey bacteria (*E. coli*)

As prey bacteria, *E. coli* (DH5 α) cells were used. To facilitate differential count and imaging, *E. coli* cells were transformed with pTurboGFP-B plasmid by heat shock method. Positive transformants were selected based on the antibiotic selection, green fluorescence and colony PCR.

Experimental set up for studying prey-predator interaction

Co-culture preparation. To test the ability of T6SS mediated predation, *C. jejuni* isolates that harbour core genes of T6SS were co-cultured with recombinant *E. coli* (DH5 α) expressing GFP (as prey). Next, co-cultured bacteria were grown at 37°C under micro-aerophilic condition (10% CO₂, 5% O₂ and 85% N₂). Samples collected at each time point were plated onto MH agar supplemented with x-gal (40 μ g/mL) (HiMedia, India) and IPTG (0.1 mM) (HiMedia, India). Finally, colonies for each type of bacteria (green colony for *E. coli* and milky white colony for *C. jejuni*) were counted and represented as CFU/mL.

Epi-fluorescence microscopy. To see the effect of prey-predator interaction on *E. coli* cells, samples collected at 7 h, were washed with PBS (pH~7.4) and fixed with 4% paraformaldehyde. Fixed cells were mounted onto a glass slide using Vecta-shield mounting media (Vector Laboratories, USA) and examined for bacterial shape and size under Axio observer microscope equipped with an ApoTome module (Carl Zeiss).

Field Emission Scanning Electron Microscopy (FESEM). To assess the effect of *C. jejuni* predation on *E. coli* morphology, Field Emission Scanning Electron Microscopy (FESEM) was performed. Briefly, co-cultured bacteria (after 5 h of co-incubation) were fixed in 2.5% (v/v) glutaraldehyde dissolved in PBS (pH~7.4) and washed thrice with PBS for 10 min. Fixed cells were then dehydrated sequentially in 35 %, 50 %, 70 %, and 95 % ethanol for 10 min followed by 1 h incubation with 100% ethanol for complete dehydration. Finally, the fixed and dehydrated samples were vacuum-dried for 1 h and fixed to aluminum stubs with silver conductive paint and sputter-coated with gold. Samples were examined using a Supra 55 Carl Zeiss scanning electron microscope.

Expression of filamenting temperature-sensitive mutant Z (*ftsZ*) gene of *E. coli*. Following co-incubation with *C. jejuni* for 7 h, *E. coli* cells were harvested by centrifugation at 6000 \times g for 10 min and washed thoroughly with PBS (pH~7.4). Total RNA was extracted by Trizol (Ambion) method following manufacturer's instruction (Invitrogen, USA). Next, approximately 1 μ g of RNA was reverse transcribed with MuLV reverse transcriptase using the Superscript Reverse Transcriptase kit (BioBharati LifeSciences Pvt. Ltd., India). To assess the relative *ftsZ* gene expression in *E. coli* cells, semi-quantitative RT-PCR was performed. All quantifications were normalized to the housekeeping gene, *16S rRNA*, using ImageLab software (Bio-Rad).

Effect of bile salt on prey-predator relation. To observe the effect of environmental stress on *C. jejuni* predation, bile salt was added in the co-culture at different concentrations (0.05%–1%, w/v). Briefly, 2.7×10^8 CFU/mL of *C. jejuni* cells was co-incubated with *E. coli* expressing GFP protein (6×10^7 CFU/mL) for 2 h. Next, a bile salt mixture (sodium cholate: 50% w/w; sodium deoxycholate: 50% w/w) (HiMedia, India) was added to the culture medium and the culture was grown for another 5 h. Next, cells were washed with fresh MH broth and plated onto MH agar plate. Colonies that appeared in the plates were then counted.

Effect of bile salt on *C. jejuni* *cmeABC* genes expression. To see the effect of bile salt induced changes in *cmeABC* transporter genes (*cmeA*, *cmeB* and *cmeC*) of *C. jejuni*, following co-incubation of *C. jejuni* and *E. coli* in the presence of bile salt (0.1%, w/v), bacterial cells were harvested by centrifugation at 6000 \times g and washed thoroughly in PBS (pH~7.4). Total RNA was extracted and the first strand cDNA was synthesized by standard method as described in the previous section. To assess the relative gene expression of *cmeA*, *cmeB* and *cmeC* in *C. jejuni*, semi-quantitative RT-PCR was performed. All quantifications were normalized to the housekeeping gene *16S rRNA*. The data presented here are the mean fold changes in *cmeA*, *cmeB*, *cmeC* and were calculated as target gene expression in bacteria cells co-cultured with *E. coli* (DH5 α) and treated with 0.1% (w/v) bile salt mixture with *C. jejuni* treated with 0.1% (w/v) bile salt mixture and *C. jejuni* without any treatment using ImageLab software (Bio-Rad).

Bile salt-induced DNA degradation of *C. jejuni*. Standard DNA smear assay (Lee et al., 2003; Bhattacharyya et al., 2017) was performed with total DNA collected from the co-culture of *C. jejuni* and *E. coli* in the absence and presence of bile salt (0.1%, w/v) as per the method described earlier with slight modification. Total DNA collected from *E. coli* in the presence of bile salt was also included in the assay and served as an internal control. The total DNA extracted from different sets was run in 0.8% (w/v) agarose gel and stained with containing EtBr (1.0 µg/mL). Gel images were captured using a gel documentation system (Bio-Rad), and intensity was measured.

Evaluation and observation of bile salt-induced intracellular ROS levels. Standard ROS quantification and imaging were performed by co-culture of *C. jejuni* in the absence or presence of bile salt (0.1%, w/v) and prey. After co-incubation for 2 h, cells were plated onto MH agar plate containing bile salt (0.1%, w/v). Colonies were then collected and suspended to an OD₆₀₀ of 0.5 in PBS followed by incubation with 20 µM of 2',7'-dichlorodihydrofluorescein diacetate (H₂DCFDA) for 45 min. Finally, the suspension was centrifuged at 8,000 ×g for 2 min to pellet the bacteria and resuspended in PBS. To measure the fluorescence signals, approximately 200 µL of aliquot was subjected for analysis using a Spectramax M2e Multi Detection Microplate Readers (Molecular Devices LLC, USA) with a 485 nm excitation filter and a 535 nm emission filter. To visualize the ROS production, cells were incubated with H₂DCFDA as mentioned earlier and then mounted onto a glass slide using Vecta-shield mounting media (Vector Laboratories, USA). Bacterial shape and size were then examined under Axio observer microscope equipped with an ApoTome module (Carl Zeiss).

Predator-prey co-incubation with bile salt. We co-incubated *C. jejuni* (2.7 × 10⁶ CFU/ mL) with *E. coli* DH5α (6 × 10⁷ CFU/ mL) and applied a low concentration of bile salt mixture (0%– 0.2%, w/v) to the prey-predator systems and kept them at 37°C at micro-aerophilic condition for 24 h. After 24 h, culture had been harvested (6000 ×g, 5 min) and washed with fresh MH broth and diluted into MH broth and plated on MH agar plate supplemented with x-gal (40 µg/mL) and IPTG (0.1 mM) and incubated at the micro-aerophilic condition at 37°C. The colony had been counted and CFU/mL was calculated.

Differential cell invasion ability of *C. jejuni*

In vitro cell invasion assay. To see the change in the ability of T6SS+ve *C. jejuni* in host cell invasion, *in vitro* cell invasion was determined by a standard gentamicin protection assay. Monolayers of human INT407 cells (3 × 10⁵/well in a 24-well tissue culture plate), were incubated with *C. jejuni* and *E. coli* at MOI 300:1 for 7 h at 5% CO₂ and 37°C in DMEM (Invitrogen) and supplemented with 10% FBS. Following incubation, the culture media was removed, and the plates were washed with PBS and cells were treated with 150 µg/mL of gentamicin (HiMedia, India) for another 2 h to kill the adhered bacteria. The infected monolayers were then lysed with 1% Triton X-100 (Sigma-Aldrich), serially diluted and plated onto MH agar. *C. jejuni* colonies that appeared on the plate were counted and presented as mean CFU/mL ± SD.

Cellular imaging of invaded bacteria. Monolayers of human INT 407 cells were treated as described in the previous section except grown in the presence of coverslips in the culture well of a 6-well plate (1.2 × 10⁶/well). Before infection, *C. jejuni* cells were stained with DAPI (5 µg/mL). Next, INT407 cells were co-incubated with the following sets of treatment groups: *C. jejuni* only, *C. jejuni*+ bile salt (0.06%, w/v), *C. jejuni* + *E. coli*, *C. jejuni*+ *E. coli*+ Bile salt (0.06%, w/v) at a total of MOI 300:1 for 7 h at under 5% CO₂ pressure. Following incubation, the culture medium was removed, and the cells were washed with PBS and treated with 150 µg/mL of gentamicin (HiMedia, India) for another 2 h to kill the adhered bacteria. After 30 min, cells were thoroughly washed and mounted onto a glass slide with Vecta-shield mounting media (Vector Laboratories, USA) for imaging. Images were viewed DAPI filter (for *C. jejuni*) with an excitation wavelength of 300–450 nm and emission wavelength of 380–650 nm. Image acquisition was done in Olympus 1X epifluorescence microscope at objective magnification 60X and processed using ImageJ software.

Mathematical analysis

Model and equations. Let $P(t)$ and $N(t)$ denote the predator (*C. jejuni*) and the prey (*E. coli*) densities respectively at an instant t . The temporal dynamics of the two populations can be described by the following set of equations,

$$\frac{dP(t)}{dt} = r_P P \left(1 - \frac{P}{K_P}\right) \quad \text{(Equation S1)}$$

$$\frac{dN(t)}{dt} = r_N N \left(1 - \frac{N}{K_N}\right) - \alpha NP \quad \text{(Equation S2)}$$

Here, r_P and r_N are the birth rates, while K_P and K_N are the corresponding carrying capacities of the predator and prey populations, respectively. In this model, when inter-species interactions are absent both the populations grow logistically and ultimately saturate to their corresponding carrying capacities. There is a predation term in Equation S2 (αNP), representing T6SS dependent killing of prey. Here, α is the coefficient of predation. We obtained closed-form analytical solutions as below:

$$P(t) = \frac{K_P P_o e^{tr_P}}{K_P + P_o e^{tr_P} - P_o} \quad \text{and}$$

$$N(t) = \frac{K_N N_o e^{tr_N} \left(-\frac{K_P - P_o}{P_o} - 1\right)^{\frac{\alpha K_P}{r_P}}}{\left[N_o e^{tr_N} \left(-\frac{K_P - P_o}{P_o} - 1\right)^{\frac{\alpha K_P}{r_P}} \left(\frac{P_o e^{tr_P}}{K_P - P_o} + 1\right)^{\frac{\alpha K_P}{r_P}} {}_2F_1\left(\frac{\alpha K_P}{r_P}, \frac{r_N}{r_P}, \frac{r_N}{r_P} + 1; -\frac{e^{tr_P} P_o}{K_P - P_o}\right) - N_o \left(\frac{P_o}{K_P - P_o} + 1\right)^{\frac{\alpha K_P}{r_P}} \left(-\frac{K_P - P_o}{P_o} - e^{tr_P}\right)^{\frac{\alpha K_P}{r_P}} {}_2F_1\left(\frac{\alpha K_P}{r_P}, \frac{r_N}{r_P}, \frac{r_N}{r_P} + 1; -\frac{P_o}{K_P - P_o}\right) + K_N \left(-\frac{K_P - P_o}{P_o} - e^{tr_P}\right)^{\frac{\alpha K_P}{r_P}} \right]}$$

Here, P_o and N_o are the initial population densities of predator and prey, respectively, and ${}_2F_1(a, b; c; x)$ denotes the hypergeometric function. These solutions were plotted in Figures 3B and 3C.

Next, in the presence of bile salt-induced stress, we extended the above model as below,

$$\frac{dP(t)}{dt} = r_P P \left(1 - \frac{P}{K_P}\right) - \beta_P c P - \beta_{int} c NP \quad \text{(Equation S3)}$$

$$\frac{dN(t)}{dt} = r_N N \left(1 - \frac{N}{K_N}\right) - \alpha NP - \beta_N c N \quad \text{(Equation S4)}$$

where, c is the bile concentration. The terms $\beta_P c P$ (for the predator) and $\beta_N c N$ (for the prey) represent their individual deaths due to the antimicrobial activity of the bile salt. The corresponding death rates are $\beta_P c$ and $\beta_N c$, respectively, which are assumed to be proportional to c . The last term ($\beta_{int} c NP$) in Equation S3 represents a 'cost of predation,' and it occurs only when a predator and prey interact with each other with a rate $\beta_{int} c$. Solving the Equations S3 and S4 in the steady-state (i.e., $\frac{dP}{dt} = 0$ and $\frac{dN}{dt} = 0$), we get the following solutions:

- $P = K_P \left(1 - \frac{\beta_P c}{r_P}\right) \equiv K'_P$, $N = 0$ (Predators exist, preys become extinct)
- $P = \frac{K_P \beta_{int} c K_N (r_N - \beta_N c) - r_N K_P (r_P - \beta_P c)}{(\alpha \beta_{int} K_P K_N c - r_P r_N)} \equiv P^*$; $N = \frac{\alpha K_P K_N (r_P - \beta_P c) - r_P K_N (r_N - \beta_N c)}{(\alpha \beta_{int} K_P K_N c - r_P r_N)} \equiv N^*$ (Coexistence)
- $P = 0$, $N = K_N \left(1 - \frac{\beta_N c}{r_N}\right) \equiv K'_N$ (Preys exist, predators become extinct)
- $P = 0$, $N = 0$ (Both become extinct)

Here, solutions (a) and (c) represent the cases where one of the populations reach a modified carrying capacity (K'_P or K'_N) while the other becomes extinct. The solution (b) represents the coexistence of both with some non-zero densities (P^* , N^*). Finally, solution (d) represents the extinction of both. Next, we discuss the conditions of stability for each solution.

Linear stability analysis

The jacobian for our system of Equations (S3 and S4), in general, is given by

$$\begin{pmatrix} \frac{\partial \dot{P}}{\partial P} & \frac{\partial \dot{P}}{\partial N} \\ \frac{\partial \dot{N}}{\partial P} & \frac{\partial \dot{N}}{\partial N} \end{pmatrix}$$

Here, $\dot{P} = \frac{dP}{dt}$ and $\dot{N} = \frac{dN}{dt}$. From this jacobian, we get two eigenvalue expressions for each of the above set of solutions (a-d). The eigenvalue expressions are:

$$\text{For } (P, N) = (K'_P, 0) : \lambda_1 = -(r_P - \beta_P c), \lambda_2 = (r_N - \beta_N c) - \frac{\alpha K_P}{r_P} (r_P - \beta_P c) \quad (\text{Equation S5})$$

$$\text{For } (P, N) = (P^*, N^*) : \lambda_1 = (r_N - \beta_N c) - 2 \frac{r_N}{K_N} N^* - \alpha P^*, \lambda_2 = (r_P - \beta_P c) - 2 \frac{r_P}{K_P} P^* - \beta_{int} c N^* \quad (\text{Equation S6})$$

$$\text{For } (P, N) = (0, K'_N) : \lambda_1 = -(r_N - \beta_N c), \lambda_2 = (r_P - \beta_P c) - \frac{\beta_{int} c K_N}{r_N} (r_N - \beta_N c) \quad (\text{Equation S7})$$

$$\text{For } (P, N) = (0, 0) : \lambda_1 = (r_P - \beta_P c), \lambda_2 = (r_N - \beta_N c) \quad (\text{Equation S8})$$

From these eigenvalue expressions, we can identify the boundaries in terms of bile salt concentrations, within which each solution would be stable. From Equation S5, we can see that the solution is stable when $c < r_P / \beta_P$ and $c < r_P (\alpha K_P - r_N) / (\alpha K_P \beta_P - r_P \beta_N)$ are satisfied simultaneously. Note that the parameters $r_N, r_P, K_N, K_P, \beta_N$ and β_P were extracted from control experiments (see Figures S3A–S3C, S6A–S6C, and Table S3), while α and β_{int} were chosen according to the best fit with the data (Figures 3C and 5C in the main text). Given these choices, we find that a critical bile salt concentration $c_1^* = r_P (\alpha K_P - r_N) / (\alpha K_P \beta_P - r_P \beta_N)$, up to which the solution (a) is stable, i.e., both the eigenvalues remain negative (see Figure S6E for eigenvalues and Figure S6D for the corresponding phase plot).

Then, from Equation S6, we get two critical bile salt concentration values, among which one is the previous c_1^* , and another is

$$c = c_2^* = \left[(\beta_{int} K_N + \beta_P) r_N - \sqrt{(\beta_{int} K_N + \beta_P)^2 r_N^2 - 4 \beta_{int} K_N K_P r_N r_P} \right] / 2 \beta_{int} K_N \beta_N$$

Between these two critical concentrations, both the eigenvalues become negative and so the coexistence solution remains stable in between the two boundaries — see Figure S6F for the phase plot at $c_1^* < c < c_2^*$ and Figure S6G for the eigenvalues corresponding to the solution(b), at different bile salt concentrations. Next, from the 3rd set of eigenvalues (Equation S7), we again get two critical bile salt concentrations, among which one is the same c_2^* and another is $c = c_3^* = r_N / \beta_N$. Between these two boundaries, solution(c) remains stable, i.e., in this regime, only prey exists and there is no predator (see Figure S6H for the phase diagram and Figure S6I for the eigenvalues corresponding to the solution(c)). Finally, from Equation S8, we obtain the condition that beyond $c = c_3^* = r_N / \beta_N$, both the eigenvalues remain negative, which reflects that neither predator nor prey will exist above this critical bile salt concentration - see Figure S6J for the phase diagram for $c > c_3^*$ and Figure S6K for the eigenvalues corresponding to the solution(d). Thus, there are four regimes that are separated by three boundaries (c_1^* , c_2^* , and c_3^*) in steady-state (as shown in Figure 5B in the main text).

QUANTIFICATION AND STATISTICAL ANALYSIS

All statistical analyses were analysed using unpaired Student's t-test when two groups were being compared using GraphPad Prism 8.0 software. All experiments were repeated as indicated in the figure legends. We consider P-value of < 0.05 as statistically significant and significance was shown as follows: ns, no significant; * $P < 0.05$; ** $P < 0.01$. Mathematical analysis was done in Mathematica software and graphs were plotted through gnuplot.

Image analysis

Cell length measurement of *E. coli* (DH5 α) was done using ZEN Digital Imaging for Light Microscopy software. Olympus 1X epifluorescence microscope images were processed in ImageJ software.